Pore-scale Microenvironments Control Anthropogenic Carbon Mineralization Outcomes in Basalt

Charles T. Depp [a*†], Quin R.S. Miller [a], Jarrod V. Crum [b], Jake A. Horner [b], H. Todd Schaef [a*]

[a] Physical and Computational Sciences Directorate, Pacific Northwest National Laboratory, Richland, Washington, 99354, USA
[b] Energy and Environment Directorate, Pacific Northwest National Laboratory, Richland, Washington, 99354, USA
[†] Current affiliation is Department of Chemistry, Colorado School of Mines, Golden, Colorado, 80401, USA

KEYWORDS: carbon sequestration, carbonate geochemistry, carbonate structure, supercritical CO_2, basalt reservoir, basalt geochemistry, geologic sequestration, climate change mitigation

ABSTRACT: Thin sections and hand samples from 50 sidewall cores from the Wallula Basalt Pilot Demonstration, a basaltic carbon sequestration demonstration, provided the opportunity for in-depth analysis carbon mineralization induced by the injection of supercritical CO_2. In this study we used optical petrography and scanning electron microscopy to characterize the physical and chemical characteristics of the basalt components influenced by carbon mineralization reactions from all available hand samples and thin sections within the three CO_2 injection zones and caprock flow interiors. We found extensive carbonate mineralization, mostly in the form of nodules that were shown to be chemically zoned; Ca-dominant in the core regions and Ca-bearing Fe-dominant in the outer regions. Carbonate mineralization also took the form of fracture filling carbonate cement and acicular aragonite were also observed. Overall, we clarified structural and paragenetic relationships between newly formed minerals, identifying a new fibro-palagonite-like, poorly crystalline silicate phase that grew on the carbonate nodules and pore-lining zeolites. We observed Fe-dominant carbonate precipitates surrounding acicular aragonite and rhombohedral Ca-carbonate cores, whereas previous studies of these zoned nodules did not observe these structures. A comprehensive accounting of the carbon mineralization products is vital to understand and predict the behavior of supercritical CO_2 in the subsurface given both the diversity of the host rock between and within injection zones, especially considering that the morphology and chemistry of the diverse precipitates and be influenced by pore-scale microenvironments of the basalt.

INTRODUCTION

The Wallula Basalt Pilot Demonstration was initiated in 2009 when an injection well was drilled into the Miocene Columbia River Basalt Group (CRBG) to a total depth of 1,253 m at a paper mill site near the town of Wallula, Washington, located in southeastern Washington State [1-4]. Within the ~828–887 m below the ground surface injection interval, were three brecciated, porous flowtop zones, that underwent extensive hydrologic characterization before CO_2 injection [2]. Zone 1 was the thickest and most porous zone and received an estimated 80% of injected CO_2, while Zone 2, being the next porous zone received and estimated 20% of injected CO_2[5]. Zone 3 had less than 1% porosity and received a comparatively miniscule amount of CO_2[5]. Zones 1, 2, and 3 are at depths of approximately 828–846 m, 854–862 m, and 866–875 m, respectively [6]. All three zones are capped by impermeable Umtanum member flows [4]. Zones 1 and 2 belong to the Indian Ridge member while Zone 3 is at the top of the Ortley member [6-8]. The basalt sequestration pilot borehole received ~977 tons of supercritical CO_2 over a 3-week period starting in August of 2013 [6, 9]. After 24 months, the well was re-entered to collect samples to be analyzed for post-injection characterization data. The samples included 50 sidewall rotary cores from the injection interval. Examination of these sidewall cores (SWC) showed amber colored, carbonate nodules that were identified as ankerite, $Ca(Fe, Mn)(CO_3)_2$ and were shown to be chemically and isotopically distinct from the naturally occurring pre-injection calcite veins [6]. These ankerite nodules are the first and only reported occurrence of anthropogenic CO_2 mineralization in basalt pores. This kind of mineralization was observed during laboratory studies [10] with CRBG samples exposed to $scCO_2$, and one of few CO_2 injection studies in the world [6, 11], which includes injection into Icelandic basalt for the CarbFix Project. Together, these endeavors are demonstrating permanent carbon storage technologies that leverages rapid reactivity in mafic formations.[12-18]

The objective of this study is to examine those sidewall cores collected post-CO_2 injection from the Wallula Basalt Pilot Demonstration and to identify the associated mineralogy. We also documented lithological features in hand samples and thin sections to better understand the paragenesis occurring post-CO_2 injection

and led to construction of a petrographic roadmap, that will help future researchers identify areas of interest and contextualize samples in a broader lithological context.

METHODS AND MATERIALS

Twenty-four sub-samples were taken from the 50 SWCs and sent to Intertek Westport Technology Center where thin sections were created. In total, 42 post-injection thin sections were created. To distinguish the carbonate composition, thin sections were stained with alizarin red S and potassium ferricyanide, causing the Ca-rich carbonate nodules to appear red and the Fe-rich to appear blue in thin section [19, 20]. All depths expressed in this paper are below the ground surface.

For this present study, thin sections and hand samples were analyzed using a Leica DMLM polarizing microscope, a Clemex motorized stage with a JS-Tango joystick and Clemex Vision Lite and PE 8.1 image analysis software, and a Nikon Optiphot2-Pol with a 0.5x C-mount adapter and a Jenoptik Gryphas AVIOR 8MP USB3 digital microscope camera with Gryphax software. Hand samples also were examined using a Wild Heerbrugg optical microscope and a Cambridge Instruments StereoZoom7. Hand samples were analyzed uncoated at low vacuum (30 Pa) in the JEOL 7001F SEM equipped with two opposing Bruker X-flash 6|60 EDS instruments. Samples were imaged using a backscattered electron detector. The EDS detectors were used to collect elemental spot analysis sample features and elemental maps were collected on the samples at an accelerating voltage of 15 kV and variable probe currents.

RESULTS

The results are presented sequentially starting with Zone 1. Each of these sections begins with the general characteristics of the host rock (i.e., porosity) and descriptions of thin section textures. This is followed by descriptions of notable minerals and cements, some of which serve as substrates for carbonate mineralization. Last, descriptions of the carbonate nodules themselves and how they fit into the broader context of the host rock are provided. This section ends with a discussion of important features regarding carbonation. A general overview of specific depths at which carbonation products were found, and the location of other important minerals commonly found in pores are represented in **Figure 1**.

Zone 1. (828–846 m) The shallowest and thickest injection zone (18 m thick) has the highest pre-injection porosity at 22% [5]. Visual inspection reveals abundant clinoptilolite and groundmass that varies in color from light gray at 828 m, down 3 m, then transitions red brown for the next 8 m, and light-dark gray in the last 7 m. Thin sections tend to have varying textures both within samples and among them. Many thin sections in Zone 1

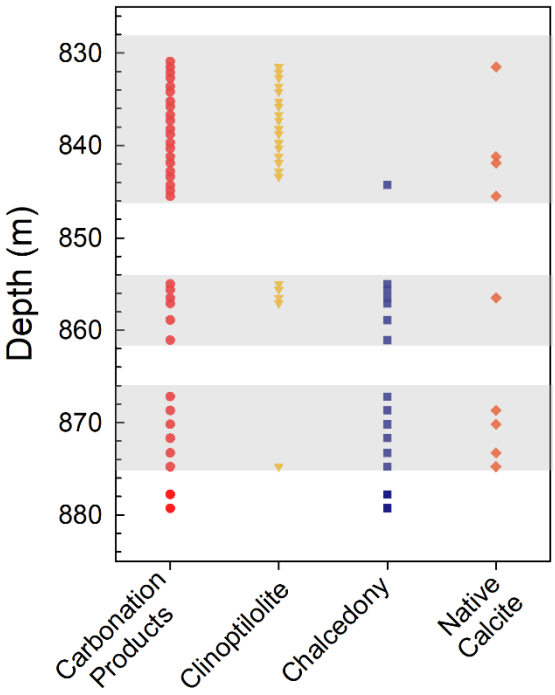

Figure 1. Overview of key minerals, including carbonation products, clinoptilolite, chalcedony (including silica spherulites) and native (naturally occurring) calcite, identified in the recovered sidewall cores. The gray areas delineate the injection zones intervals.

contain multiple distinct textures, such as the sample from 837.3 m, seen in **Figure S1**. The multi-textured samples in Zone 1 typically range from hypocrystalline regions, where the dominant phenocryst is plagioclase in a matrix dominated by glass, to cryptocrystalline where plagioclase is also dominant, but inequigranular, anhedral pyroxene is more common in this texture. The cryptocrystalline, intersertal groundmass is often an altered brown or red color, possibly due to devitrification or other alteration. These regions typically contain large plagioclase grains, small plagioclase grains, intersertal glass and small, relatively equigranular opaque minerals. The samples with the most heterogeneous textures are those from depths of 831.5, 832.7, 836.7, 837.3, 838.8, and 842.8 m. The rest are comparatively homogenous, and contain only one texture, which can generally be described as being comprised mostly of inequigranular plagioclase and pyroxenes, often contain opaque minerals and some glass. Plagioclase is the dominant phenocryst in almost all textures (most are subophitic or nesophitic) and typically is subhedral to anhedral, relatively equigranular in regions dominated by glass and inequigranular elsewhere. Some plagioclase grains are oikocrysts, containing Fe- and Ca–rich carbonate inclusions. Plagioclase-hosted carbonate inclusions are found in all three injection zones but are most common

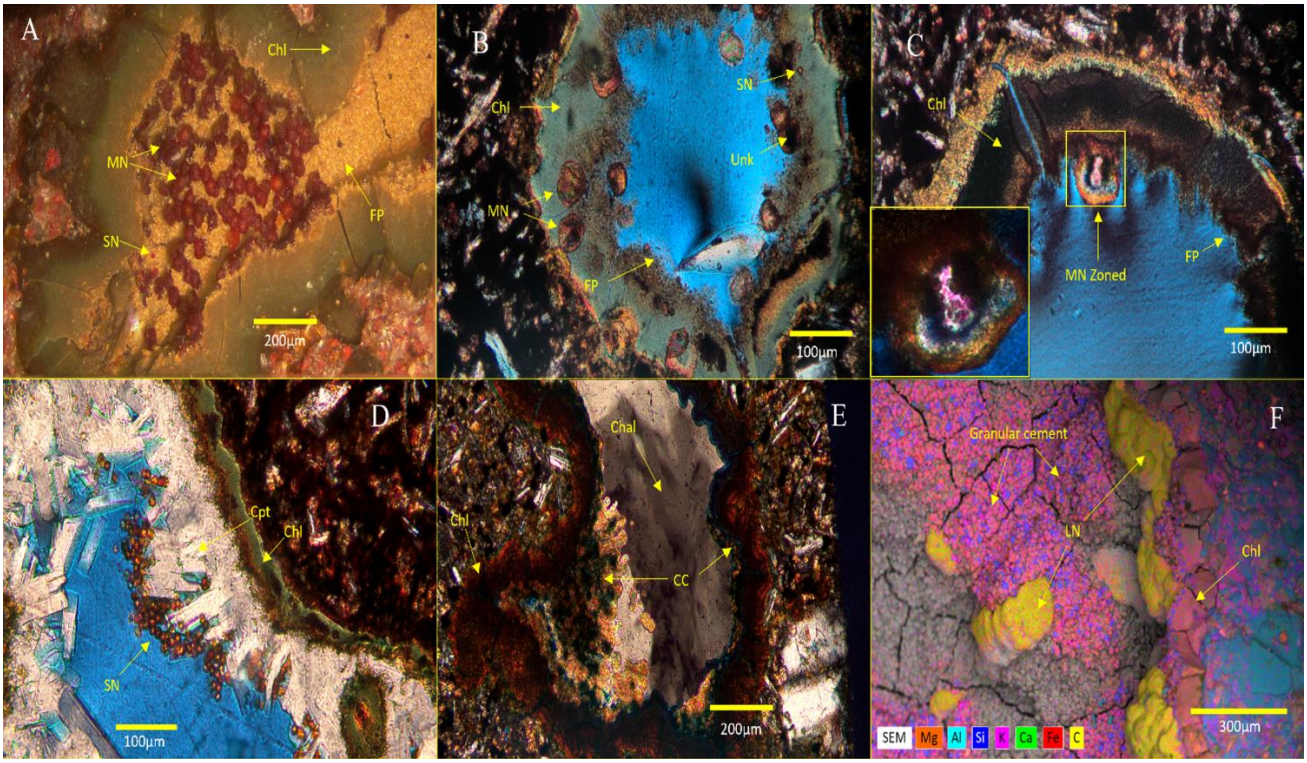

Figure 2. A: (835.8 m). Optical image of small and medium red carbonate nodules and small orange carbonate nodules growing on fibro-palagonite (light green) in a chlorophaeite (dark green) coated pore. **B:** (835.2 m). Thin section PPL image of medium and small carbonate nodules growing in pores. **C:** (835.2 m). Thin section XPL image of a medium carbonate nodule exhibiting zoning. **D:** (832.7 m). Thin section PPL image of clusters of small carbonate nodules growing on clinoptilolite. **E:** (844.3 m). Thin section XPL image of Fe and Ca rich carbonate cement and chalcedony cement. **F:** (844.3 m). SEM image and EDS mapping of oblong carbonate nodules on granular cement. (SN = small carbonate nodule, MN = medium carbonate nodule, LN = large carbonate nodule, FP = fibro-palagonite, Unk = unknown, CC = carbonate cement, Chal = chalcedony, Chl = chlorophaeite, Cpt = clinoptilolite)

in Zone 3 (**Figure S2**). Within Zone 1, carbonate nodules were not observed above 831.5 m or below 845.5 m.

In Zone 1, the most common cements found growing from the edges of pores, and even entirely filling small pores, are green and green-brown chlorophaeite as seen in **Figure 2A**. On top of the chlorophaeite is a layer of fibro-palagonite (light green) and carbonate nodules (red and brown). In this paper, chlorophaeite refers generally to the chemically variable, clay mineral-like, green, yellow and brown, cement that is an alteration product that often coats pores and also is found in the groundmass of many samples and in all zones [21]. We use the term fibro-palagonite to specify a granular mat-like phase that is sometimes found growing on chlorophaeite [22, 23]. The chlorophaeite, which is rich in Mg, Fe, Si, and Al, according to EDS data (**Table S2-S4**), is present from a depth of 831.5 m down 10.7 m. The chlorophaeite in samples shallower than 835.2 m tends to be thinner. Between 835.2 m and 838.8 m, it is thicker and zoned with a thin outer brown layer followed by a thick inner green layer. In hand samples the chlorophaeite of different samples look nearly identical, although there are differences that are more easily distinguished in thin sections. **Figure 2B-E** demonstrate this variability. Cross polarized light (XPL) and plane polarized light (PPL) images of **2B-E** all show the many colors and textures found in Zone 1, from the thick green cement of **2B**, thick zoned cement of **2C**, the thin green cement of **2D** and the brown cement of **2E**. The samples at depths 839.7 m and 840.3 m have a thin cement that is yellow-brown in hand samples, but turquoise colored in thin sections in both XPL and PPL images. At depths from 841.9 m through 843.4 m, there is a thin gray-green cement that, in thin sections, is like the cement observed in the thin section from 839.7 m. The hand sample from 841.9 m also has a light green cement that fills small pores throughout the groundmass. The pores in the sample at depths of 844.3 m were coated with a thick brown layer of chlorophaeite and many of them are filled with chalcedony. In thin section, it is apparent that there is both an Fe-rich Ca-rich carbonate cement layer between the brown chlorophaeite and the chalcedony in many of the pores. The hand sample from 845.5 m was not very porous but did contain green chlorophaeite in a fracture, and some red-brown cement that potentially may be a carbonation product.

Clinoptilolite is ubiquitous throughout much of Zone 1 as one of the most common minerals growing in pores that is not a cement. In some samples, such as those from 835.8, 842.8 and 843.4 m, it dominates an estimated

50 and 75% of the pores. It is most abundant in samples at depths of 835.8, 839.7–840.3, and 842.8–843.4 m, and is at very low abundance at 841.2 m and practically nonexistent in Zone 1 beneath 843.4 m. It generally grows on chlorophaeite, and other pore coating cements as can be seen in **Figure 2D**, not directly on the groundmass. In pores where it is not present, there is often the yellow-green, fibro-palagonite mentioned earlier. This material is especially abundant from depths of 832.1 m down to 835.8 m, but it also is found throughout the next 3 m of depth beneath that. It does not appear to be more abundant than clinoptilolite in any sample in Zone 1. In some samples, such as the one from 833.6 m, they occur together, but this is not common. Generally, the fibro-palagonite is observed growing on top of the clinoptilolite as shown in **Figure S3**. It is also worth noting that some fibro-palagonite appears to be growing on the carbonate nodules as well as can also be seen in **Figure S3-S4,** indicating the reprecipitation of this phase was induced by CO_2.injection.

Chalcedony is present in Zone 1 in the sample from 844.3 m, where it takes the form of pore filling chalcedony, and silica spherulites. In the thin section, shown in **Figure 2E**, the pores are coated with dark brown chlorophaeite, and most are filled with chalcedony and both Ca- and Fe-rich carbonate cement. In some pores, the carbonate cement and chalcedony appear intergrown, while in others the carbonate cement is between the chlorophaeite and chalcedony. In some clusters of carbonate nodules, there is also a granular form of SiO_2 per EDS that may be a coprecipitate (**Figure 3B**).

The carbonate nodules in this zone are abundant yet small compared to other zones, yet still exhibit a wide range of sizes, colors, and habits. In general, they tend to range from small, orange, and vitreous, to medium, dark red, and dull, with many intermediates between these two endmembers (i.e., small, and red or medium and orange). The only hand sample with carbonate nodules that can be observed unaided was from 844.3 m. In Zone 1 the Ca- to Fe-rich zoning is not really visible in the small carbonate nodules, possibly due to their size (if it even occurs at all) but can be observed in some medium-sized nodules such as the one in **Figure 2C**. In the center of the nodule is the characteristic pink color shown by Ca-rich carbonate minerals, followed by blue colors as the Fe becomes the dominant cation. The carbonate nodules occur in three size groups: small, medium, and large. The diameters of the small nodules are <35 µm , the medium nodules are <200 µm and the large are ≥200 µm. The distinction between small and medium initially was made to distinguish extremely small nodules that often grew with the zeolite mineral clinoptilolite from larger nodules that tended to grow in pores without clinoptilolite.

Pores dominated by fibro-palagonite are often observed with many medium, red, opaque carbonate nodules on them. Other sizes and colors also grow on it but are more difficult to see (**Figure S5**). **Figure 2A** shows a pore surface with medium-sized reddish carbonate nodules on top of the light green pore-lining fibro-palagonite. **Figure 2B** is a PPL image of medium and some small carbonate nodules growing on chlorophaeite, with what appears to be fibro-palagonite. The only carbonate nodules that commonly grow on clinoptilolite are small, orange, and vitreous (**Figure S6**) and are usually either dispersed throughout, or growing in botryoidal clusters as in **Figure 2D**. The average carbonate nodule size in this cluster is approximately 8.8 µm, and most are Ca-rich (based on dye, not EDS). This can be observed at depths of 838.8 and 831.5 m but are found throughout the shallower half of this zone.

There were some unique morphologies observed in this zone. The large carbonate nodules from 844.3 m have a unique shape. They are represented in the yellow-orange color in the EDS chemical map in **Figure 2F**. They have an elongate shape, botryoidal texture, are composed of many carbonate nodules and are growing on a granular cement composed of silica spherulites and other silicate minerals that contain Mg, and Fe (**Table S5**). In some samples, such as shown in **Figure 3A**, the carbonate material looks like an intermediate between a nodule and cement. In **Figure 3A**, the circular looking material appears to be flattened or smeared together in

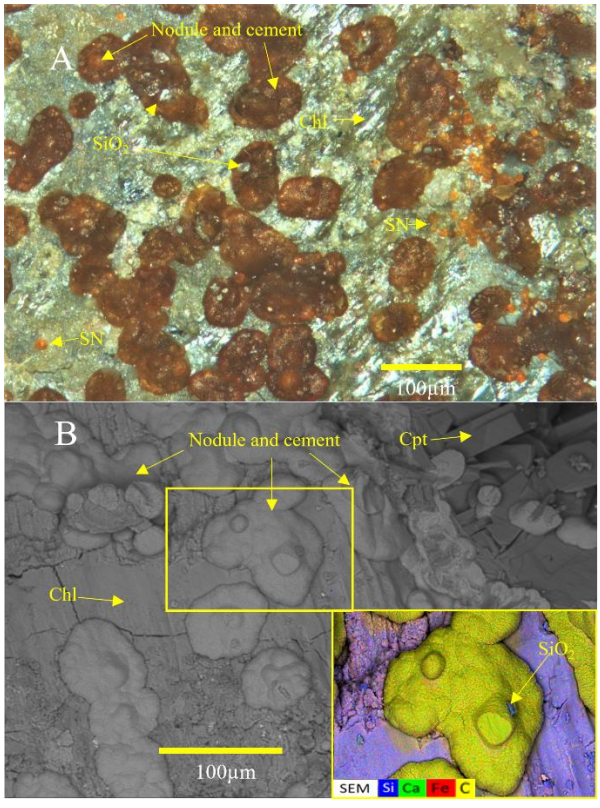

Figure 3. **A:** (838.2 m). Optical image of small and medium carbonate nodules exhibiting a morphology that is a mix of cement and nodules. **B:** (838.2 m). SEM image of cement/carbonate nodule morphology and an EDS chemical map. Abbreviations here are the same as in **Figure 2**.

some places, similar to a "pancake" siderite morphology.[24, 25] In some examples, carbonate nodules can be seen growing from the circular smear. These nodules tend to be red to orange in color, and measurements of 131 of these carbonate nodules/cements revealed a mean diameter of 60 μm, with a minimum and maximum of 25 and 111 μm respectively. **Figure 3B** is an SEM image and EDS map of the morphology shown in **Figure 3A**. The Ca- and Fe-rich carbonate material is represented by the yellow color, while the chlorophaeite is purple. This material is common from depths of 838.8 m and shallower.

Calcite also was found in Zone 1, particularly in the thin section from 831.5 m and the hand sample from 841.9 and 843.4 m. It is unclear whether this calcite was naturally occurring, however, the calcite from the hand sample from 841.9 m had some red carbonate cement on its edges, so it must have occurred before the carbonation products associated with the project (**Figure S7**).

Zone 2. (854–862 m) Zone 2 has a thickness of 8 m and a pre-injection porosity of 13% [5]. The samples in this zone are less obviously altered than the samples from Zone 1. Most samples from 856.5 m to the bottom of the zone are a light gray color, and the groundmass in the corresponding thin sections are very homogenous with little alteration compared to samples from 855.6 and 855 m and those from Zone 1. Overall, the Zone 2 thin sections are relatively homogenous except for the samples from 855.6 and 855 m (**Figure S1**). The thin sections from 855 m have three different textures, all of which are hypocrystalline; however, two are composed mostly of glass and the other has some cryptocrystalline matrix. Of the two composed of glass, they can be distinguished by color, one has a red hue (that is visible on the thin section itself) and the other is black. The mineralogy of these two textures is nearly identical, with plagioclase being the main phenocryst, with some pyroxenes present. The third texture has only intersertal glass on a gray-brown matrix. The cements in the pores also vary with different textures. At 855.6 m, there are two different matrices distinguished by either red or black colors. There are mostly small subhedral to anhedral plagioclase and pyroxene grains dispersed throughout the groundmass. The rest of the thin sections are very homogenous and almost identical to each other in terms of mineralogy. They consist of large and small plagioclase grains with interstitial pyroxene, and opaque minerals, also intersertal glass and brown chlorophaeite. No carbonate nodules were found below depths of 861.1 m.

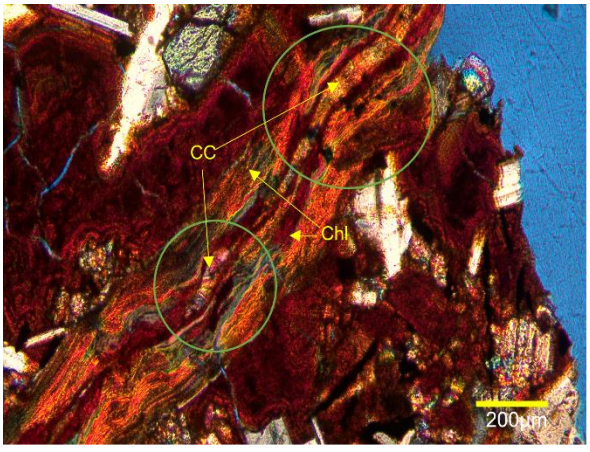

Figure 4. (858.9 m). Thin section PPL image of a fracture containing carbonate cements in the green circles. Abbreviations here are the same as in **Figure 2**.

There are cements similar to those found in Zone 1, although there are also many instances of unique cement. At depths of 855 m and 855.6 m, there is a darker green, almost turquoise cement. In the corresponding thin section for the sample taken at 855 m, this cement is bright green and vibrant in XPL and PPL, although in the red, glassy region, the cement is duller and thicker. Overall, the hand sample from 855.6 m is not ideal for most notable features are on the side of the sample where the core was cut so the features are difficult to see. The corresponding thin section for this sample contains a unique material. The pore spaces are mostly filled with some material that is opaque in XPL and exhibits a range of different colors in PPL. The hand sample from 856.5 m has a cement that is like the thick brown cement found at 844.3 m and is found growing around chalcedony likewise. The hand sample from 857.1 m has a cement that is turquoise but shows zoning. The outside is yellow, and in some cases, there is another yellow layer on the inner most part. For PPL in thin section, the yellow layer is very visible. In both XPL and PPL, the cement is a bright blue color that is unique to this sample. The sample from 858.9 m is not very porous compared to the other samples, however there are some fractures, most of which are filled with multiple materials that are easily distinguished in thin section. The outer-most part of the fracture is a layer of chalcedony, followed by some other cement that, in thin section, is bright green and orange in XPL and PPL. Finally in the center of the fracture (in some sections) is a carbonate cement that has regions of that are Fe-rich and some that are Ca-rich (**Figure 4**). In the thin section there are also regions where carbonate cement is found intergrown with chalcedony.

Clinoptilolite is abundant at 855 m and is similar to Zone 1 in this regard; however, the rest of Zone 2 generally has less clinoptilolite than most Zone 1 samples. From 855 m, the general trend is a decrease in clinoptilolite with depth to 858.9 m where none was observed in either hand sample or thin section. At 855.6 m there is a small amount that can be seen in the hand sample, but none was observed in thin section, possibly due to the yellow cement dominating most pores. A large amount of the pore space in the 856.5 m hand sample is dominated by chalcedony; although, in thin section, clinoptilolite grains present in the same pores look like the chalcedony grew around them. The hand sample does

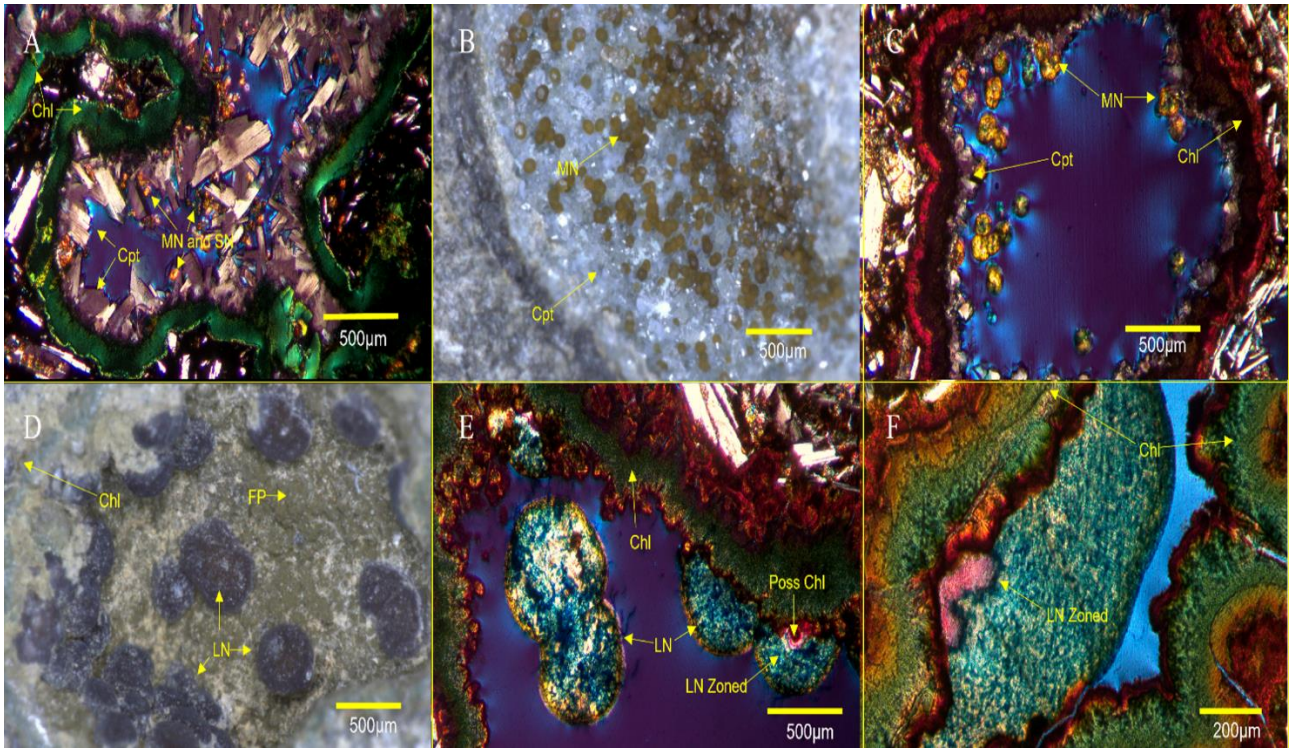

Figure 5. A: (855 m). Thin section XPL image of medium carbonate nodules growing in clinoptilolite on a unique vibrant green cement. **B:** (856.5 m). Optical image of medium carbonate nodules growing in a clinoptilolite dominated pore. **C:** (856.5 m). Thin section XPL image of medium carbonate nodules and clinoptilolite. **D:** (857.1 m). Optical image of large carbonate nodules growing in pores with fibro-palagonite. **E** and **F:** (857.1 m) Thin section XPL and PPL images (respectively) of large carbonate nodules growing in pores. Zoning is especially visible in F. Abbreviations here are the same as in **Figure 2**.

contain a few pores that are dominated by clinoptilolite, but there are also a few large pores that contain only fibro-palagonite. The hand sample from 855.6 m is the first one that appears to contain more fibro-palagonite than clinoptilolite.

The sample from 855 m possibly has the most diverse size distribution of carbonate nodules of the entire project area (**Figure S8**). There are small and medium carbonate nodules, growing individually and in clusters, usually in the same pores as clinoptilolite as can be seen in **Figure 5A**. Some medium carbonate nodules grow around clinoptilolite grains and some exhibit zoning. Large carbonate nodules also are present, but typically grow by themselves or with other large nodules in open pores without clinoptilolite. Most of the carbonate nodules observed in the hand sample are medium and small and orange and brown in color. In the hand sample from 855.6 m, there are what look like medium and small carbonate nodules that range in color from orange to dark red, but this is difficult to tell because of the issue with the hand sample mentioned earlier. No carbonate nodules were observed in the corresponding thin section. Almost all carbonate nodules from 856.5 m are visible unaided. The carbonate nodules that grow in the clinoptilolite pores, as seen in **Figure 5B** and **C**, are mostly medium-sized and grow in clusters and individually, although compared to most of the carbonate nodules observed in Zone 1 are still massive. The largest carbonate nodules are found in a pore containing brown-yellow fibro-palagonite. The carbonate nodules here are brown to orange in color. The carbonate nodules growing in the fibro-palagonite, which can be seen in **Figure 5D** and **E** are darker than the ones growing in clinoptilolite, which are more orange in color and appear slightly less opaque. In thin section, it appears the carbonate nodules are more likely to grow on chlorophaeite that is light brown or green, compared to chalcedony and clinoptilolite that grow mostly on brown chlorophaeite. The sample from 857.1 m has carbonate nodules that are comparable in size to those taken at 856.5 m. The large carbonate nodules here grow almost exclusively on fibro-palagonite. There also are some very small, orange carbonate nodules in the fibro-palagonite; however, these are difficult to see given the nature of the substrate and the size of the nodules.

Chemical zoning in these larger carbonate nodules, such as shown in **Figure 5F**, is much easier to observe and is common in most of the large nodules. Medium carbonate nodules in Zone 2 show chemical zoning more commonly than in Zone 1, where a small number of nodules exhibit chemical zoning, some are ambiguous, and others do not appear to be chemically zoned at all.

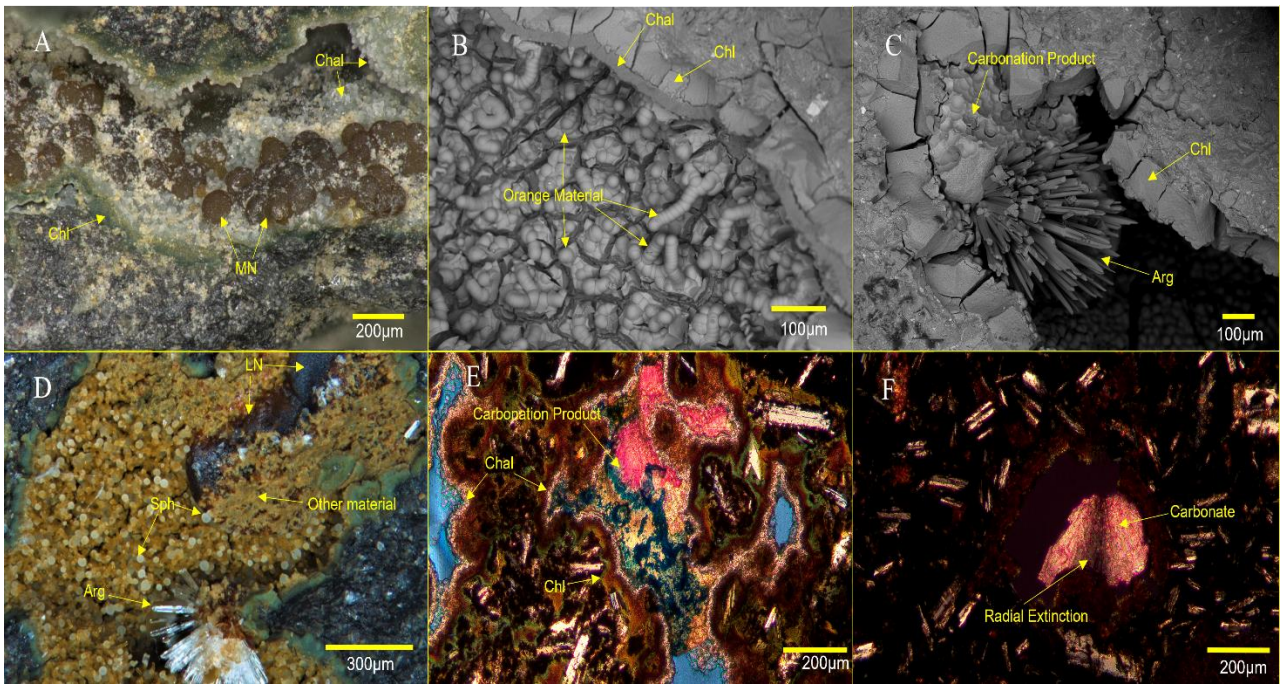

Figure 6. **A:** (870.2 m). Optical image of medium carbonate nodules covered in drilling mud (tan) growing on botryoidal chalcedony cement. **B:** (873.3 m). SEM image of orange, vitreous cement growing in a pore. **C:** (873.3 m). SEM image of one instance of aragonite. **D:** (870.2 m). Optical image of semi-spherical carbonate nodules with silica spherulites and some tan material growing on the open face and another instance of aragonite. **E:** (870.2 m) Thin section PPL image of an oddly shaped carbonation product **F:** (873.3 m). Thin section XPL image Ca-rich carbonate material that is angular and has a radial extinction. (Sph = silica spherulite). Other abbreviations are the same as in **Figure 2**.

In the hand sample, there is a clinoptilolite-bearing pore with small and medium carbonate nodules ranging in color from orange to dark red, and many of the nodules are covered and enveloped in a tan cement (**Figure S9**) that has not been identified. The hand sample from 858.9 m is much less porous than shallower samples, and only contained clusters of small, orange carbonate nodules that appear to grow in the fractures, but most carbonate material was the cement mentioned earlier. No carbonate nodules were observed in this thin section, only cement.

Zone 3. (866–875 m) Zone 3 has a thickness of 9 m and a pre-injection porosity of 1% [5]. This zone has a unique variety of cements and accessory features not found in any of the other zones. Overall, this zone appears to have experienced more alteration than Zone 2. This degree of alteration is apparent on the mostly red hand sample from 867.2 m but is much more apparent in many of the thin sections that appear mottled and have matrices of varying colors. Plagioclase is once again the dominant phenocryst. Like Zone 1, many of the samples exhibit multiple textures, ranging from mostly glass to mostly altered, cryptocrystalline groundmass, with intersertal glass; however, overall, the texture mostly is hypocrystalline. Samples from shallower depths (867.2 and 870.2 m) contain the most glass and contain very little pyroxene. Large grains of plagioclase also are rare. Samples from 873.3 and 874.8 m are much more crystalline. Those samples contain pyroxene and large grains of plagioclase are much more common. Samples from 887.8 m are almost entirely crystalline, with some intersertal glass and opaque minerals present.

In the hand sample from 867.2 m, there is a light green cement. Additionally, there is a gray-white botryoidal chalcedony cement that is also present in samples through 874.8 m. At a depth of 1.5 m lower, there are three different cements: a dark green pore-coating cement that is present through the sample at 871.7 m, the same gray-white botryoidal chalcedony mentioned above, and the same light green cement (**Figure 6A**). In thin section, the green cement is a bright lime green in both XPL and PPL, with undulose extinction. At 873.3 m, most pore-lining cement is relatively thin, brown chlorophaeite that is dark brown in XPL and light brown in PPL, but there is also the spherulitic chalcedony cement. There is an orange translucent, vitreous material that grows on top of the chalcedony in some areas. SEM revealed that this material is composed of a layer of small carbonate nodules. They display a unique morphology where they are growing on top of one another into the pore space and have a worm-like texture to them as seen in **Figure 6B** (chemical data shown in **Table S7**). There is a similar looking material in the sample from 874.8 m (**Figure S10**). At this same depth, there are thin brown, and yellow cements, also clinoptilolite can be found

growing in pores and fractures. This is the only sample in Zone 3 in which clinoptilolite was found. Silica spherulites were observed growing among the clinoptilolite grains in thin section.

The area from 870.2 m to the bottom of the zone is one of the most chalcedony and silica rich regions in the entire target area and is distinct from most of the chalcedony and silica observed in other zones. Here, it is coating the insides of pores and is botryoidal and spherulitic chalcedony, in contrast to the silica observed, for example, in samples from around 856.5 m. In that region, chalcedony tends to fill the pores in such a way that the original orientation of the rock can be distinguished. In the thin section from 858.9 m, there is an instance of silica spherulites and the hand sample for 855 m has botryoidal chalcedony cement, but it is significantly less abundant.

Four instances of aragonite also were found in hand samples in this zone (**Figure 6C** and **D**): three from the sample from 870.2 m and one from 873.3 m. In all four instances there are other carbonation products growing on and around the aragonite grains (**Table S6**). We believe that the aragonite is anthropogenic in origin, as the occurrence of aragonite in basaltic carbonation reactions has been demonstrated in laboratory experiments [26].

In both the hand sample and thin section from 867.2 m, there are filamentations algal-bacterial features that are yellow-brown in the hand sample and opaque in the thin section. There also are relatively large pieces of semi-transparent naturally occurring calcite in samples from 868.7 m and 870.2 m. In the thin section, the calcite is pink, large, and tabular and fills fractures and vesicles. On some edges, there are Fe-rich carbonate nodules that have grown on the calcite. Almost all the calcite grains go extinct at the same angle, denoting that they have the same crystallographic orientation.

In terms of size, the carbonate nodules in Zone 3 are more like in Zone 2 than those in Zone 1. In the sample from 867.2 m, there are large, brown, spherical minerals found in the red groundmass of the sample that look like carbonate nodules, but EDS revealed them to be a ferromagnesian silicate instead. Large, dark red carbonate nodules were found growing around the algal/bacterial filaments as can be seen in (**Figure S11**). This also can be observed in the thin section. There also are smaller carbonate nodules here, found growing on the light green cement. The sample from 870.2 m has large, dark red carbonate nodules, many of which are half-formed semi-spheres, and some even have silica spherulites and another mineral growing on the flat, unformed half as can be seen in **Figure 6D** (additional photos in **Figure S12** and other chemical data in **Table S8**). At 873.3 m, there are a few large carbonate nodules in the hand sample, most of which have grown on the botryoidal chalcedony, but the bulk of the carbonate material is more easily examined in thin section. The carbonate nodules have a light orange-brown color, and almost appear to have an inner gray-white portion in the center, but that is difficult to say for sure.

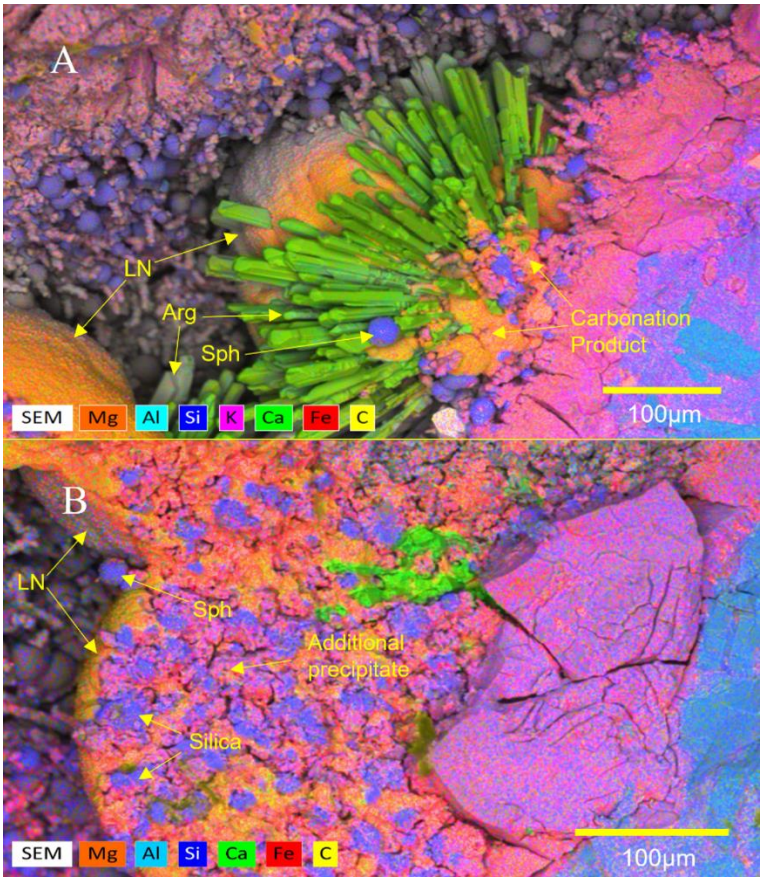

Figure 7. **A:** (870.2 m). SEM image and EDS chemical map of two instances of aragonite and carbonate nodules in a pore. Silica spherulites grow on and between aragonite crystals, possibly a product of the carbonation reaction. **B:** (870.2 m). SEM image and EDS map of a semispherical carbonate nodule with silica spherulites, Si-rich material and some other Fe-, Mg-, and Si-rich material growing on top of it. Abbreviations here are the same as in **Figure 2**.

Zone 3 contains some unique morphologies that are exclusive to this zone and best observed in the thin sections (**Figure S13**). Here, however, most of the pore space looks more like irregular, angular fractures as shown in **Figure 6E**. There are many instances of Ca-rich, carbonate material (no outer Fe-rich area) that fill entire small fractures. However, some of this material has a radial shape rather than the tabular shape observed in the native (naturally occurring) calcite but unlike the

typical rounded nodules observed elsewhere, it has angular edges (**Figure 6F**). When the stage is rotated, some of this material exhibits radial extinction, and in other instances, it appears to be composed of many crystals that all go extinct at different angles. Although the origin of these Ca-rich carbonates is unclear, previous laboratory based basalt carbonation experiments did produce calcites with a radiating texture [26]. There are also rounded, Fe-rich carbonate nodules in these samples, and in some instances these nodules are attached to the ends of, or intergrown with, the pink carbonate material (e.g., the sample from 870.2 m).

DISCUSSION

Key Findings. Each zone contained unique carbonation products (although there were similar products as well) that distinguish them from each other. One apparent difference between zones is the disappearance of botryoidal clusters of small carbonate nodules commonly observed in Zone 1 as depth increases. There are few of these clusters observed in Zones 2 and 3, although clusters of medium-sized carbonate nodules were observed in all zones. On the other hand, there are no large carbonate nodules observed in Zone 1 thin sections and only one hand sample in which they were observed (844.3 m). In Zone 1 only small carbonate nodules tend to grow in the same pores as clinoptilolite, while medium and small carbonate nodules in the same sample will grow on pores with fibro-palagonite. The circular smears of **Figure 3** along with some other products in **Figure S5**, only tend to grow in specific samples, on specific green chlorophaeite and not on fibro-palagonite or clinoptilolite. This green chlorophaeite cement found in much of the shallower half of this Zone 1 appears to be the best surface for growing a variety of different carbonate nodules and carbonate cement in Zone 1. The oblong carbonate nodules from 844.3 m are another example. These carbonate nodules grow on a granular cement composed of silica spherulites and some other material (**Figure S5)** that is unique to that sample.

In order to understand the behavior of CO_2 in the subsurface it is important to identify any co-precipitates that formed during carbonation. In Zone 1 it is common to find small silica-rich materials growing on or near carbonate nodules, and can be seen in **Figure 3A** and **B**. Another instance of possible carbonate and silica co-precipitation in Zone 1 are the carbonate cements in the sample from 844.3 m, in which the carbonate cement appears closer to the edge of the pore, suggesting it may have occurred first, and in some cases, it even appears to be intergrown. In Zone 2, small and medium carbonate nodules appear to be covered or enveloped in a tan cement mentioned earlier. In Zone 3, silica spherulites and other Si-rich material is observed to be growing around the aragonite and carbonate nodules (**Figure 7A**). As mentioned in the ***Zone 3*** section, we believe the aragonite to have formed before the carbonate nodule, and there are silica spherulites present on both. There are also large carbonate nodules that are half formed with silica spherulites and some other tan-colored material growing on its unformed face, shown in **Figure 7B**, providing evidence that the reaction is producing silica from reacting with the basalt mass.

In all three flow top targets there are carbonate nodules that exhibit chemical zoning. In thin section it appears that this is not a gradual change, and the Ca-rich centers can be seen with a distinct line of blue dye around its edges, beyond which no more pink is observed. There appears to be no blending of the two in most cases. There are some rare instances in Zones 2 and 3 where there does appear to be a purple color that could represent a transition area. It is not clear if zoning occurs at all in small carbonate nodules, but it is visible in many of the medium nodules although most visible in the large ones. The small, clustered carbonate nodules in Zone 1, appear to be overwhelmingly red in color (**Figure 2D**). In the EDS data seen in **Figure 3B** it appears there is an even distribution of Fe and Ca throughout, with no anomalous concentrations observed. The blue carbonate nodules may be zoned and, therefore just difficult to see. Some medium and, in some cases, large carbonate nodules also show only one color. Medium carbonate nodules can be

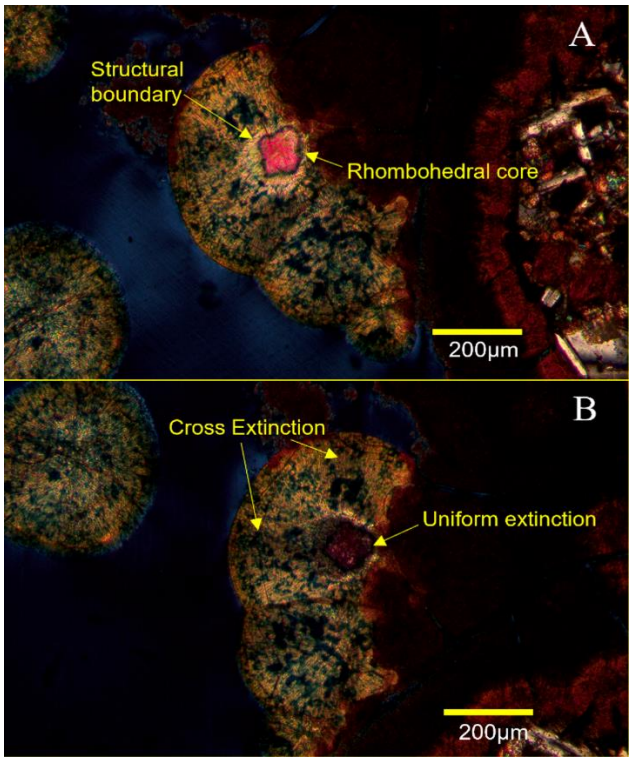

Figure 8. **A:** (856.5 m). Thin section XPL image of a large carbonate nodule positioned 45 degrees from extinction to show the rhombohedral shape of the core and the structural boundary. **B:** The same carbonate nodule, rotated to show extinction features (cross extinction in outer Fe-rich area, uniform extinction in the core).

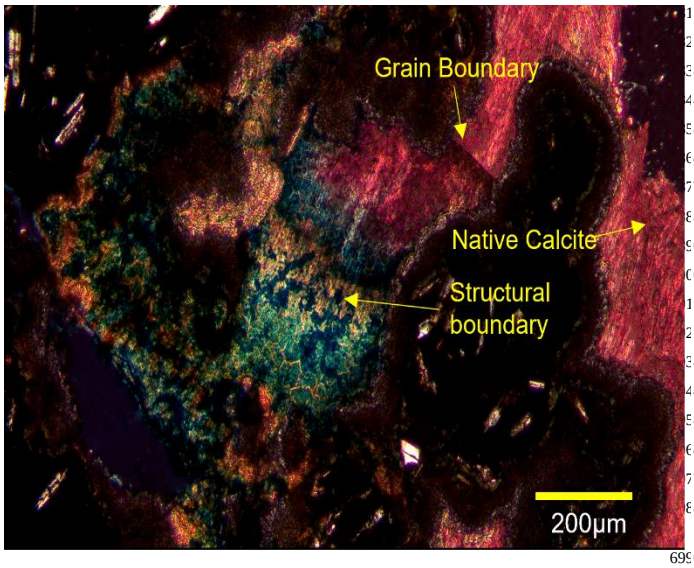

Figure 9. (870.2 m). Thin section XPL image of a carbonate nodule growing on a native calcite grain.

either entirely blue or entirely red (**Figure 2B**), while large ones have been observed to be only blue. For the large and medium blue carbonate nodules, this could just be the result of how the thin section was cut and the fact that the dye is only surficial [20].

The Ca-rich portion of chemically zoned carbonate nodules exhibit a range of morphologies themselves. Many of them, and a small part of the Fe rich region that immediately surrounds it that makes up the core of the carbonate nodule, often appear to be rhombohedral in shape (**Figure 8A** and **Figure S16**), or an irregular shape. The differences in shape may likely arise from how the thin sections were cut, and it is possible that they are all relatively rhombohedral. Other than rhombohedral cores, aragonite also sometimes serves as the Ca-rich core around which the Fe-dominated carbonate grows. This can be observed in SEM in **Figure 6C** and **Figure 7A** and in thin section in **Figure S15**. Aragonite cores appear far less common than rhombohedral cores, with only one instance being observed in thin section compared to countless instances of rhombohedral cores. There is a difference in optical extinction between the core and outer portions that can be observed in chemically zoned carbonate nodules. The core (Ca-rich and inner Fe-rich area) exhibits uniform extinction, suggesting that it is one crystal, or possibly multiple large crystals all oriented in the same direction (**Figure 8B**). The outer Fe-rich parts, on the other hand, typically exhibit undulose extinction, although it can sometimes be difficult to see at all; extinction crosses can also be exhibited (**Figure 8B**). Overall, this suggests that the outer part of the carbonate nodule is crystallographically distinct from the core. The extinction crosses suggest they have a spherulitic texture, which is composed of radially oriented crystallites [27, 28], suggestive of rapid growth at supersaturated conditions[29, 30]. This texture can be observed in thin section (**Figure S17**) and SEM images (**Table S5** and **Table S6**). **Figure 9** is an excellent example of the structural and compositional diversity the carbonate nodules exhibit. The larger Ca-rich region on the right is a piece of native calcite. The grain boundary between the carbonate nodule and the calcite is visible, and when rotated, the Ca-rich part of the carbonate nodule, and the inner Fe-rich part go extinct with the larger calcite grain, possibly representing syntaxial growth with that grain and a similar crystal lattice (unlike the products growing on non-carbonate substrates), or identical mineral phase, and the rest of the outer carbonate nodule exhibits extinction crosses. This may suggest that regardless of what the specific mineral identity of the Ca-rich core is, the Fe-rich carbonate crystallites still show a tendency to grow from them.

Comparisons with previous studies. Each zone was unique regarding its physical characteristics as well as mineralogical makeup and degree of alteration. Each zone also yielded unique carbonation products as mentioned earlier. It seems likely that controls are exerted by the host rock that influences the size, shape and composition of the carbonation products. Studies of carbonate morphologies and growth in soils have shown a dependence on matrix composition and texture, and particularly the amount of clay in the environment [31]. It also has been shown that the presence of specific clays, such as montmorillonite and other smectites, can affect the nucleation, growth, and even the specific phase of $CaCO_3$ that precipitates[32, 33, 34]. It is possible that similar effects occur in basalts with different textures and compositions, especially given the abundance of clay mineral-like chlorophaeite from prior alteration which varies, sometimes significantly, from sample to sample (and also within the same samples) (**Figure S14**). It's also been shown in lab experiments that cation substitution varied between different basalts (i.e., Deccan flood basalt and CRBG) and also that some samples had distinct chemical boundaries, some had none at all and others had gradual compositional changes [35]. . The porosity of the host rock is also highly variable between zones, which could also influence nucleation and growth. One important feature of a geologic carbon storage project is injectivity, which is directly related to the thickness and permeability of the host rock[36]. Zone 1, being the thickest and most permeable zone, received most of the injected CO_2 and as mentioned earlier, had a tendency toward abundant, small and medium carbonate nodules compared to the other zones. Some models of nucleation and growth in a porous media show higher initial concentrations can have lower inductions times[37]. Other models have found higher reservoir conductivity can significantly increase carbonate mineralization in basalt[38]. It is possible due to the higher concentrations, that there was a period of rapid nucleation, followed by

transport of CO_2 further from the inlet and hence no opportunity for larger nodules to grow.

Some experimental data shows and stoichiometric models predict that silica as well as aluminosilicates are produced in carbonation reactions with basalt[15, 26, 39-42]. Therefore, the co-precipitation of silica and other materials observed in several instances in all three zones suggests that the supercritical CO_2 did react with and dissolve the host rock, rather than just precipitating out of solution or from dissolving and reprecipitating preexisting carbonate minerals.

Carbonate minerals associated with carbonation of basalts that have distinct chemical boundaries are not unique and have been observed in multiple laboratory studies[35, 42, 43]. It is also important to note the non-zoned, Ca-rich carbonates of Zone 3. Although they are unique among the three zones, Ca-rich carbonates like calcite were found experimentally in multiple laboratory carbonation reactions and were also reported by Carbfix[16, 40, 44]. The unique feature of these carbonates seems to be the structural heterogeneities observed in large and medium carbonate nodules. These structural features haven't been reported in other experiments or from field data and appear to be unique to this project. Just as the changing composition could track changes in the pore fluid composition, the spherulitic texture also may suggest some sort of change in the environment as well [45, 46].

Additional Considerations and Future Research.

Additional research is also needed to understand the structural heterogeneities of many of the carbonate nodules. Although we know the chemical composition of the different regions, understanding the exact mineral identities of the crystallites that make up the outer Fe-rich region, may be important in understanding how conditions change as the reactions proceed.

It was noted earlier that algal/bacterial filaments were found in Zone 3. Although we collected no data on this subject, it would be useful to understand possible interplay between biological and inorganic components in the basalt. It is known that mafic reservoirs can host diverse microbial biospheres[47] and it has been shown experimentally that organic acids can affect the type, extent and rates of carbon mineralization outcomes through complexation[48] Microbes can have complex interactions with CO_2 injections that may be advantageous or deleterious depending on the ecosystem[49], but are important to understand in order to maximize mineralization efficiency and for potential selection of injection sites. Our group is actively investigating biomineralization in basaltic carbon storage settings.

CONCLUSION

Post-injection analysis of thin sections and hand samples from the Wallula Basalt Pilot Demonstration has revealed extensive carbonate mineralization throughout the target zones. Although carbonation products were identified in each zone, there were many differences between them regarding morphology, size, and abundance of products. It is quite possible that the chemical and physical variations of the zones are responsible for the different carbonation products. Structural and chemical heterogeneities of the carbonate nodules may also hold information on how the carbonation reaction effects the host rock and pore fluid and vice versa. The goal of this study was to examine all available samples, catalog all carbonation products in the context of the host rock, and increase our understanding of the fate of supercritical CO_2 in the subsurface. With increasing interest in using basalt for carbon sequestration[50 51], it is important to collect as much data as possible from existing demonstrations. This study will aid researchers in parameterizing models for future and possibly commercial carbon sequestration projects.

ASSOCIATED CONTENT

Supporting Information

Depths at which samples were collected (Table S1); Additional XPL and PPL thin section photographs (Figures S1, S2, S4, S7, S8, S11, S13, S14, S15, S16, and S17); Additional hand sample photographs (Figures S3, S5, S6, S9, and S12); SEM images and EDS data (Tables S2, S3, S4, S5, S6, S7 and S8 and Figure S10)

Abbreviations

- Arg: Aragonite
- CC: Carbonate cement
- Chal: Chalcedony
- Chl: Chlorophaeite
- Cpt: Clinoptilolite
- CRBG: Columbia River Basalt Group
- FP: Fibro-palagonite
- LN: Large carbonate nodule
- MN: Medium carbonate nodule
- PPL: Plane-polarized light
- SN: Small carbonate nodule
- Sph: Silica spherulite
- Unk: Unknown
- XPL: Cross-Polarized Light

Supplemental Information

AUTHOR INFORMATION

Corresponding Authors

*Corresponding Authors

Charles T. Depp, ctdepp@mines.edu

H. Todd Schaef, todd.schaef@pnnl.gov

Notes

The authors declare no competing financial interests.

ORCID
C.T. Depp: 0000-0002-7763-4066
Q.R.S. Miller: 0000-0003-3009-9702
J. V. Crum: 0000-0001-9197-0878
J.A. Horner: 0000-0003-4418-0675
H.T. Schaef: 0000-0002-4546-3979

ACKNOWLEDGEMENTS

This work was performed at the Pacific Northwest National Laboratory (PNNL) and was supported by the U.S. Department of Energy's Carbon Storage Program. We acknowledge support from Darin Damiani (DOE HQ) and the Carbon Utilization and Storage Partnership (CUSP). CTD was partially supported by the U.S. Department of Energy, Office of Science, Office of Workforce Development for Teachers and Students (WDTS), under the Science Undergraduate Laboratory Internships Program (SULI) at PNNL. QRSM was partially supported by the U.S. Department of Energy (DOE), Office of Science, Office of Basic Energy Sciences (BES), Chemical Sciences, Geosciences, and Biosciences Division through its Geosciences program at the Pacific Northwest National Laboratory (PNNL). We would like to thank the two anonymous reviewers whose insightful comments helped improve our article. We appreciate their time and attention. We also thank Dr. Ross Cao (PNNL) for a helpful review of an earlier draft.

REFERENCES

1. McGrail, B. P.; Spane, F. A.; Sullivan, E. C.; Bacon, D. H.; Hund, G. In *The Wallula Basalt Sequestration Pilot Project*, 10th International Conference on Greenhouse Gas Control Technologies, Amsterdam, Netherlands, Sep 19-23, 2010; Amsterdam, Netherlands, 2010; pp 5653-5660.
2. McGrail, B. P.; Sullivan, C. E.; Spane, F. A.; Bacon, D. H.; Hund, G.; Thorne, P. D.; Thompson, C. J.; Reidel, S. P.; Colwell, F. S., Preliminary Hydrogeologic Characterization Results from the Wallula Basalt Pilot Study. In Pacific Northwest National Laboratory: Richland, WA PNWD-4129, 2009.
3. McGrail, B. P.; Sullivan, C. E.; Spane, F. A.; Bacon, D. H.; Hund, G.; Thorne, P. D.; Thompson, C. J.; Reidel, S. P.; Colwell, F. S., Preliminary Hydrogeologic Characterization Results from the Wallula Basalt Pilot Study, PNWD-4129. In PNNL: Richland, Wahsington, 2009.
4. McGrail, B. P.; Spane, F. A.; Sullivan, E. C.; Bacon, D. H.; Hund, G., The Wallula Basalt Sequestration Pilot Project. *Energy Procedia* **2011,** *4*, 5653-5660.
5. White, S. K.; Spane, F. A.; Schaef, H. T.; Miller, Q. R. S.; White, M. D.; Horner, J. A.; McGrail, B. P., Quantification of CO-$_2$ Mineralization at the Wallula Basalt Pilot Project. *Environmental Science & Technology* **2020,** *54*, (22), 14609-14616.
6. McGrail, B. P.; Schaef, H. T.; Spane, F. A.; Cliff, J. B.; Qafoku, O.; Horner, J. A.; Thompson, C. J.; Owen, A. T.; Sullivan, C. E., Field Validation of Supercritical CO_2 Reactivity with Basalts. *Environ. Sci. & Technol. Lett.* **2017,** *4*, (1), 6-10.
7. Reidel, S. P.; Tolan, T. L., The Grande Ronde Basalt, Columbia River Basalt Group. *Geological Society of America Special Papers* **2013,** *497*, 117-153.
8. Reidel, S. P.; Spane, F. A.; Johnson, V. G. *Natural gas storage in basalt aquifers of the Columbia Basin, Pacific Northwest USA: A guide to site characterization*; Pacific Northwest National Lab.(PNNL), Richland, WA (United States): 2002.
9. McGrail, B. P.; Spane, F. A.; Amonette, J. E.; Thompson, C. R.; Brown, C. F., Injection and Monitoring at the Wallula Basalt Pilot Project. *Energy Procedia* **2014,** *63*, 2939-2948.
10. McGrail, B. P.; Schaef, H. T.; Ho, A. M.; Chien, Y. J.; Dooley, J. J.; Davidson, C. L., Potential for carbon dioxide sequestration in flood basalts. *Journal of Geophysical Research-Solid Earth* **2006,** *111*, (B12).
11. Matter, J. M.; Stute, M.; Snaebjornsdottir, S. O.; Oelkers, E. H.; Gislason, S. R.; Aradottir, E. S.; Sigfusson, B.; Gunnarsson, I.; Sigurdardottir, H.; Gunnlaugsson, E.; Axelsson, G.; Alfredsson, H. A.; Wolff-Boenisch, D.; Mesfin, K.; Taya, D. F. D.; Hall, J.; Dideriksen, K.; Broecker, W. S., Rapid carbon mineralization for permanent disposal of anthropogenic carbon dioxide emissions. *Science* **2016,** *352*, (6291), 1312-1314.
12. Qomi, M. J. A.; Miller, Q. R. S.; Zare, S.; Schaef, H. T.; Kaszuba, J. P.; Rosso, K. M., Molecular-Scale Mechanisms of CO_2 Mineralization in Nanoscale Interfacial Water Films. *Nature Reviews Chemistry* **2022,** *6*, 598–613.
13. Snæbjörnsdóttir, S. Ó.; Sigfússon, B.; Marieni, C.; Goldberg, D.; Gislason, S. R.; Oelkers, E. H., Carbon dioxide storage through mineral carbonation. *Nature Reviews Earth & Environment* **2020,** *1*, (2), 90-102.
14. Tutolo, B. M.; Awolayo, A.; Brown, C., Alkalinity Generation Constraints on Basalt Carbonation for Carbon Dioxide Removal at the Gigaton-per-Year Scale. *Environ. Sci. Technol.* **2021,** *55*, (17), 11906-11915.
15. Xiong, W.; Wells, R. K.; Menefee, A. H.; Skemer, P.; Ellis, B. R.; Giammar, D. E., CO2 mineral trapping in fractured basalt. *International Journal of Greenhouse Gas Control* **2017,** *66*, 204-217.
16. Xiong, W.; Wells, R. K.; Horner, J. A.; Schaef, H. T.; Skemer, P. A.; Giammar, D. E., CO_2 Mineral Sequestration in Naturally Porous Basalt. *Environ. Sci. & Technol. Lett.* **2018,** *5*, (3), 142-147.
17. Wells, R. K.; Xiong, W.; Giammar, D.; Skemer, P., Dissolution and surface roughening of Columbia River flood basalt at geologic carbon sequestration conditions. *Chem. Geol.* **2017,** *467*, 100-109.
18. Menefee, A. H.; Giammar, D. E.; Ellis, B. R., Permanent CO_2 Trapping through Localized and Chemical Gradient-Driven Basalt Carbonation. *Environ. Sci. Technol.* **2018,** *52*, (15), 8954-8964.
19. Dickson, J. A. D., Carbonate identification and genesis as revealed by staining. *Journal of Sedimentary Research* **1966,** *36*, (2), 491-505.
20. Dickson, J. A. D., A Modified Staining Technique for Carbonates in Thin Section. *Nature* **1965,** *205*, (4971), 587-587.

21. Peacock, M. A.; Fuller, R. E., Chlorophaeite, sideromelane and palagonite from the Columbia River Plateau. *American Mineralogist* **1928,** *13*, (7), 360-383.
22. Stroncik, N. A.; Schmincke, H.-U., Palagonite – a review. *International Journal of Earth Sciences* **2002,** *91*, (4), 680-697.
23. Stroncik, N.; Schmincke, H., Evolution of palagonite: Crystallization, chemical changes, and element budget. *Geochemistry Geophysics Geosystems* **2001,** *2*.
24. Antoshkina, A. I.; Ryabinkina, N. N.; Valyaeva, O. V., Genesis of siderite nodules from the lower carboniferous terrigenous sequence in the Subpolar Urals. *Lithol. Mineral Resour.* **2017,** *52*, (2), 111-124.
25. Antoshkina, A. I.; Ryabinkina, N. N. In *Lower Carboniferous Siderites: A Product of Bottom Seeps and Bacterial Metanogenesis (Subpolar Urals)*, 2018, Springer: pp 139-142.
26. Schaef, H. T.; McGrail, B. P.; Owen, A. T., Basalt Reactivity Variability with Reservoir Depth in Supercritical CO_2 and Aqueous Phases. *Energy Procedia* **2011,** *4*, 4977-4984.
27. Sun, C.-Y.; Gránásy, L.; Stifler, C. A.; Zaquin, T.; Chopdekar, R. V.; Tamura, N.; Weaver, J. C.; Zhang, J. A. Y.; Goffredo, S.; Falini, G.; Marcus, M. A.; Pusztai, T.; Schoeppler, V.; Mass, T.; Gilbert, P. U. P. A., Crystal nucleation and growth of spherulites demonstrated by coral skeletons and phase-field simulations. *Acta Biomaterialia* **2021,** *120*, 277-292.
28. Beck, R.; Andreassen, J.-P., Spherulitic Growth of Calcium Carbonate. *Crystal Growth & Design* **2010,** *10*, (7), 2934-2947.
29. De Yoreo, J. J.; Gilbert, P. U. P. A.; Sommerdijk, N. A. J. M.; Penn, R. L.; Whitelam, S.; Joester, D.; Zhang, H.; Rimer, J. D.; Navrotsky, A.; Banfield, J. F.; Wallace, A. F.; Michel, F. M.; Meldrum, F. C.; Cölfen, H.; Dove, P. M., Crystallization by particle attachment in synthetic, biogenic, and geologic environments. *Science* **2015,** *349*, (6247).
30. Spencer, E., On some occurrences of spherulitic siderite and other carbonates in sediments. *Quarterly Journal of the Geological Society* **1925,** *81*, (1-4), 667-705.
31. Wieder, M.; Yaalon, D. H., Effect of matrix composition on carbonate nodule crystallization. *Geoderma* **1974,** *11*, (2), 95-121.
32. Kralj, D.; Vdović, N., The influence of some naturally occurring minerals on the precipitation of calcium carbonate polymorphs. *Water Research* **2000,** *34*, (1), 179-184.
33. Fodor, M. A.; Ható, Z.; Kristóf, T.; Pósfai, M., The role of clay surfaces in the heterogeneous nucleation of calcite: Molecular dynamics simulations of cluster formation and attachment. *Chemical Geology* **2020,** *538*, 119497.
34. Molnár, Z.; Pekker, P.; Dódony, I.; Pósfai, M., Clay minerals affect calcium (magnesium) carbonate precipitation and aging. *Earth and Planetary Science Letters* **2021,** *567*, 116971.
35. Schaef, H. T.; McGrail, B. P.; Owen, A. T., Carbonate mineralization of volcanic province basalts. *International Journal of Greenhouse Gas Control* **2010,** *4*, (2), 249-261.
36. Raza, A.; Rezaee, R.; Gholami, R.; Bing, C. H.; Nagarajan, R.; Hamid, M. A., A screening criterion for selection of suitable CO2 storage sites. *Journal of Natural Gas Science and Engineering* **2016,** *28*, 317-327.
37. Fazeli, H.; Masoudi, M.; Patel, R. A.; Aagaard, P.; Hellevang, H., Pore-Scale Modeling of Nucleation and Growth in Porous Media. *ACS Earth and Space Chemistry* **2020,** *4*, (2), 249-260.
38. Liu, D.; Agarwal, R.; Li, Y.; Yang, S., Reactive transport modeling of mineral carbonation in unaltered and altered basalts during CO2 sequestration. *International Journal of Greenhouse Gas Control* **2019,** *85*, 109-120.
39. Olajire, A. A., A review of mineral carbonation technology in sequestration of CO_2. *Journal of Petroleum Science and Engineering* **2013,** *109*, 364-392.
40. Raza, A.; Glatz, G.; Gholami, R.; Mahmoud, M.; Alafnan, S., Carbon mineralization and geological storage of CO2 in basalt: Mechanisms and technical challenges. *Earth-Science Reviews* **2022,** *229*, 104036.
41. Polites, E. G.; Schaef, H. T.; Horner, J. A.; Owen, A. T.; Holliman, J. E.; McGrail, B. P.; Miller, Q. R. S., Exotic Carbonate Mineralization Recovered from a Deep Basalt Carbon Storage Demonstration. *Environmental Science & Technology* **2022**.
42. Kanakiya, S.; Adam, L.; Esteban, L.; Rowe, M. C.; Shane, P., Dissolution and secondary mineral precipitation in basalts due to reactions with carbonic acid. *J. Geophys. Res. Solid Earth* **2017,** *122*, (6), 4312-4327.
43. Gysi, A. P.; Stefánsson, A., Mineralogical aspects of CO2 sequestration during hydrothermal basalt alteration — An experimental study at 75 to 250°C and elevated pCO2. *Chemical Geology* **2012,** *306-307*, 146-159.
44. Clark, D. E.; Oelkers, E. H.; Gunnarsson, I.; Sigfússon, B.; Snæbjörnsdóttir, S. Ó.; Aradóttir, E. S.; Gíslason, S. R., CarbFix2: CO2 and H2S mineralization during 3.5 years of continuous injection into basaltic rocks at more than 250 °C. *Geochimica et Cosmochimica Acta* **2020,** *279*, 45-66.
45. Shtukenberg, A. G.; Punin, Y. O.; Gunn, E.; Kahr, B., Spherulites. *Chemical Reviews* **2012,** *112*, (3), 1805-1838.
46. Beck, R.; Andreassen, J.-P., The onset of spherulitic growth in crystallization of calcium carbonate. *Journal of Crystal Growth* **2010,** *312*, (15), 2226-2238.
47. Lavalleur, H. J.; Colwell, F. S., Microbial characterization of basalt formation waters targeted for geological carbon sequestration. *FEMS microbiology ecology* **2013,** *85*, (1), 62-73.
48. Miller, Q. R.; Kaszuba, J. P.; Schaef, H. T.; Bowden, M. E.; McGrail, B. P., Impacts of organic ligands on forsterite reactivity in supercritical CO2 fluids. *Environmental Science & Technology* **2015,** *49*, (7), 4724-4734.
49. Trias, R.; Ménez, B.; le Campion, P.; Zivanovic, Y.; Lecourt, L.; Lecoeuvre, A.; Schmitt-Kopplin, P.; Uhl, J.; Gislason, S. R.; Alfreðsson, H. A.; Mesfin, K. G.; Snæbjörnsdóttir, S. Ó.; Aradóttir, E. S.; Gunnarsson, I.; Matter, J. M.; Stute, M.; Oelkers, E. H.; Gérard, E., High reactivity of deep biota under anthropogenic CO2 injection into basalt. *Nature Communications* **2017,** *8*, (1), 1063.
50. Arvanitis, A.; Koutsovitis, P.; Koukouzas, N.; Tyrologou, P.; Karapanos, D.; Karkalis, C.; Pomonis, P., Potential Sites for Underground Energy and CO2 Storage in Greece: A Geological and Petrological Approach. *Energies* **2020,** *13*, (11).

51. Shrivastava, J.; Rani, N.; Pathak, V., Geochemical modeling and experimental studies on mineral carbonation of primary silicates for long-term immobilization of CO2 in basalt from the eastern Deccan volcanic province. *Jour. Indian Geophys. Union, Sp* **2016,** *1*, 42-58.